We are IntechOpen, the world's leading publisher of Open Access books Built by scientists, for scientists

4,800
Open access books available

122,000
International authors and editors

135M
Downloads

Our authors are among the

154
Countries delivered to

TOP 1%
most cited scientists

12.2%
Contributors from top 500 universities

CLARIVATE ANALYTICS BOOK CITATION INDEX INDEXED

WEB OF SCIENCE™

Selection of our books indexed in the Book Citation Index in Web of Science™ Core Collection (BKCI)

Interested in publishing with us?
Contact book.department@intechopen.com

Numbers displayed above are based on latest data collected.
For more information visit www.intechopen.com

13

Infrared Lasers in Nanoscale Science

Rui F. M. Lobo[1,2]
[1]*Group for Nanoscale Science and Nanotechnology (GNCN), Physics Department, Faculdade de Ciencias e Tecnologia - New University of Lisbon, Caparica,*
[2]*Institute for Science and Technology of Materials and Surfaces (ICEMS)*
Portugal

1. Introduction

In the nearly half a century scientists have already realized that, just as Feynman predicted, there is plenty of research room at the bottom of the matter world in a tiny universe so small that new methods for viewing it are still being discovered. Actually, nanoscience and nanotechnology have evolved into a revolutionary area of technology-based research, opening the door to precise engineering on the atomic scale and affecting everything from healthcare to the environment. Nanoscience research and education lead to nanotechnology, the manipulation of nanometer-length atoms, molecules, and supramolecular structures in order to generate larger structures with superior features. Because all natural materials and systems exist at a nanoscale level, nanotechnology impacts a variety of scientific fundamental and applied disciplines, from physics to medicine and engineering. Nanomaterials consisting of nano-sized building blocks exhibit unique and often superior properties relatively to their bulk counterpart. Due to the fact that most of the novel properties of nanomaterials are size-dependent, synthesis methods leading to better control of size, distribution and chemical content of the nanoparticles are imperative in modern nanotechnologies.

On its turn, the laser has been one of the top applied physics inventions that played a significant role in many fields of science and technology. It has been used in tackling and solving many scientific and technological problems, including interesting applications in the field of nanotechnology, biotechnology/medicine, environment, material characterization, and energy.

There are several gaseous molecules which serve as good laser media and the majority of them are simple molecules which provide emission in the ultraviolet. Infrared molecular gas lasers fall into two general categories, namely the middle- and far-infrared lasers, which occur on rotational-vibrational transitions or on pure rotational transitions.

The N_2 laser is known as a pulse ultraviolet laser and in addition it covers some lines in the infrared up to 8,2 μm. Normally, the pulse width is a few nanoseconds and a high-voltage power supply of 30-40 kV is necessary to excite it. The HF is a high power chemical laser media with an emission wavelength of about 2,7 μm, a laser pulse of the order of μs in duration and the output energy ranges from 1 J to more than 1 kJ per pulse. The DF and HBr chemical lasers emit larger wavelengths than the HF laser, and their output power is lower [1,2].

The CO_2 laser is a gas laser electrically pumped, that emits in the mid-infrared. It gives a cw output at 10 μm in the infrared with a high efficiency and it is the most practical molecular laser. There are a large number of CO_2 lasers, varying in structure, method of excitation and capacity, which can provide hundreds of laser lines, the main ones being between 9 and 11 μm. The output power of even a small CO_2 laser is about 1 kW and large ones give over 10 kW. The usual way of obtaining single-line oscillation is to use a diffraction grating in conjunction with a laser resonator. If only mirrors are used, simultaneous oscillation on several lines in the neighborhood of 10,6 μm is commonly obtained [1,2]. Transverse excited atmosphere (TEA) CO_2 lasers have a very high (about atmospheric) gas pressure. As the voltage required for a longitudinal discharge would be too high, transverse excitation is done with a series of electrodes along the tube. TEA lasers are operated in pulsed mode only, as the gas discharge would not be stable at high pressures, and are suitable for average powers of tens of kilowatts [1,2].

Although N_2O and CO laser have a lower output power than the CO_2 laser, they have about one hundred laser lines each in the ranges 10-11 μm and 5-6,5 μm, respectivelly (considering the main isotopic species). The molecules NH_3, OCS, CS also have quite a few laser lines in the infrared. With the SO_2, HCN, H_2O, many laser lines are obtained in the infrared from 30 μm up to submilimeter wavelengths [1,2].

Dye lasers are convenient tunable lasers in the visible but not so far in the infrared, mainly due to the lack of appropriate dyes, and in addition, since the dye laser medium is liquid, it is very inconvenient to handle.

In face of the real advantage of the laser as a very intense heating source that can be applied to a very small area, the most significant areas in which the CO_2 laser has shown remarkable applications are in the general fields of materials processing and medical applications. This includes cutting, cauterizing, drilling, material removal, melting, welding, alloying, hardening, surgery, cancer treatment and so forth.

The carbon dioxide laser, invented by Patel [3], operates on rotational-vibrational transitions and is still one of the most useful among all the infrared molecular lasers. In general, it is one of the most powerful lasers currently available. It operates in the middle infrared wavelength region with the principal wavelength bands centering around 9.4 and 10.6 micrometers. It is also quite efficient, with a ratio of output power to pump power as large as 20%. It can operate at very high pressures because the energies of the upper laser levels are much closer to the ground state of the CO_2 molecule than are energies of the upper laser levels of atomic lasers and so the electron temperature can be much lower, thereby allowing higher operating gas pressures. Higher operating gas pressures means a much greater population in the upper laser level per unit volume of the laser discharge and therefore much higher power output per unit volume of laser gain media. These lasers have produced cw powers of greater than 100 kW and pulsed energies of as much as 10 kJ. The gain occurs on a range of rotational-vibrational transitions that are dominated by either Doppler broadening or pressure broadening, depending upon the gas pressure.

Although laser radiation is obtainable with pure CO_2 gas, the usual CO_2 laser uses a mixture of He, N_2 and CO_2. The population inversion in the laser is achieved by a sequence of fundamental processes starting by vibrational excitation of nitrogen molecules in the electric discharge. The nitrogen molecules are left in a lower excited state and their transition to

ground state takes place by collision with cold helium atoms. The resulting hot helium atoms must be cooled in order to sustain the ability to produce a population inversion in the carbon dioxide molecules. In sealed lasers, this takes place as the helium atoms strike the walls of the container. In flow-through lasers, a continuous stream of CO_2 and nitrogen is excited by the plasma discharge and the hot gas mixture is exhausted from the resonator by pumps.

The CO_2 laser transitions are the 961 cm^{-1} transition of the 10,4 μm band and the 1064 cm^{-1} transition of the 9,4 μm band. Owing to the symmetry of the CO_2 molecule, laser transitions occur to lower energy levels whose rotational quantum numbers are even, resulting in more than 30 laser lines in each of the two branches P and R [1,2].

In general, there are two common different types of CO_2 laser configurations. In one of them (longitudinally excited laser), the CO_2 laser is excited by direct current and when the pressure raised from 10^3 Pa to 10^4 Pa, a peak power is obtainable by using a pulsed discharge. This is an arc maintained by an anode and a cathode at the ends of a long discharge tube. Another possibility is the transversely excited atmospheric pressure laser (TEA), excited by an arc discharge at roughly atmospheric pressure [4]. The current in the arc flows at right angles to the axis of the laser [5]. A TEA laser is always pulsed and many CO_2 lasers are TEA lasers.

Some CO_2 TEA lasers have been developed with additional techniques enabling us to achieve tuneable wavelengths, and in particular may reach oscillation threshold for several atomic or molecular transitions. The laser can then simultaneously oscillate on these transitions. In order to reach single mode operation, one has to first select a single transition.

Because the laser transitions are actually on vibration-rotation bands of a linear triatomic molecule CO_2, the rotational structure of the P and R bands can be selected by a tuning element in the laser cavity. Because transmissive materials in the infrared are rather lossy, the frequency tuning element is almost always a diffraction grating. By rotating the diffraction grating, a particular rotational line of the vibrational transition can be selected. The finest frequency selection may also be obtained through the use of an etalon.

A procedure towards optimization performance of a CO_2 pulsed tuneable laser was developed which allows the power and the energy to be optimized [5]. The MTL3-GT is a very compact grating tuneable TEA laser version (Figure 1), and represents a significant improvement in performance and portability [6]. Combining a pulse mode with a grating tuning facility, it enables us to scan the working wavelength between 9.2 and 10.8 μm (operating on more than 60 lines), with repetition rates ranging from single-shot to 200 Hz. The maximum energy for this version is 50 mJ/pulse on the strongest lines. The MTL3-GT CO_2 infrared laser works with a a gas mixture (40% He : 30% CO_2 : 30% N_2) and a chiller for high repetition rates. Actually, above 20 Hz, the number of HV discharges increases and the laser needs to be cooled down in order to lower the temperature in the optical cavity.

Following an adequate procedure, the energy values could be optimized in intensity and stability, and therefore indirectly laser power. In addition, the same procedure allows to check the wavelengths of the laser emission lines in the absence of a spectrometer, using a previously established conversion table of the grating position versus line designation. With such method, many experiments can be performed in real time with simultaneous control of

power/energy and wavelength, and taking advantage of the full laser power for each selected wavelength.

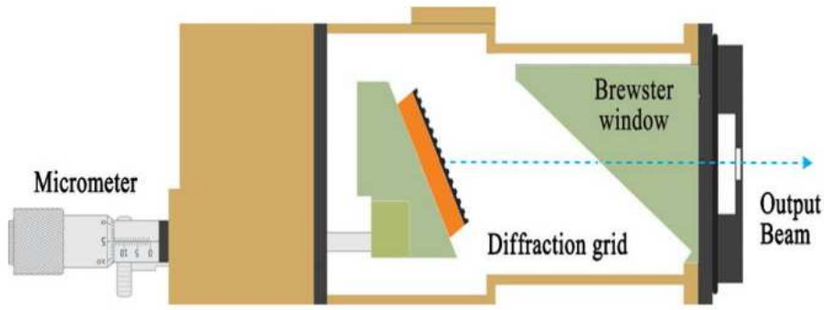

Fig. 1. Schematics of the MTL3-GT TEA laser from Edinburgh Instruments [6]

One could observe, after improving the procedure, that energy values are more stable in all four emission bands (9P, 9R, 10P and 10R). This behaviour was also observed regardless of the repetition rate, even for higher ones around 100 Hz. Besides energy, power was also measured and improved following the same procedure. This procedure can also be used on other infrared lasers with some minor adaptations regarding the software and energy detectors used.

In order to overcome several error sources which are the causes of non-reproducibility in these type of lasers, the procedure used a continuous measurement of the energy line, making use of an infrared detector and power meter acquisition software. Such a display method reflects the inherent error associated with the grating tuning motion and therefore the micrometer hysteresis. The method is suitable to obtain the energy and power values for each emission laser TEA CO_2 line optimized. The experimental set-up consists of the tuneable TEA CO2 laser, a pyroelectric energy detector connected to a handheld power/energy meter and a computer for acquisition purposes [5].

Since the laser is tuneable by wavelength, some specific emission lines of the CO_2 molecule can be selected, making use of a micrometer. The correspondence between such emission lines and the micrometer driving position can be previously verified with an infrared spectrometer, in order to check those mentioned in the user's manual. Changing the position of the micrometer, one varies the angular position of the diffraction grid. This allows to scan among several emission lines, and so to choose the working wavelength.

Using a graphite target block, the pulse shape can be observed while the micrometer is moving. When the correct position is achieved, the focus should be round and symmetric (≈5 mm in diameter), displaying a strong luminosity and without sudden changes for consecutive shots. However, this method proved to be somewhat inaccurate and not very user friendly. To overcome these drawbacks, one must look at the real-time graphic line display of energy on the computer and follow its behaviour during the micrometer rotation, as well. The higher value of the energy line display corresponds, for each wavelength, to the desired position of the micrometer. This can be confirmed at any time by crossing the laser beam with the graphite target [5]. However, the micrometer hysteresis makes the procedure

unreliable, tedious and very sensitive to the rotation speed of the micrometer and stability of the energy signal. Thus, two acquisitions were made for each repetition rate, one by turning the micrometer clockwise and another counter clockwise. An average of them was calculated and definitive energy values were registered. This procedure was repeated in the opposite direction, in order to obtain an average, and also to confirm the reproducibility of the result. It was actually confirmed for every emission line and several values of repetition rates [5].

Acquisitions recorded without concerns about the external factors and in different days revealed instability in energy values for each repetition rate measured (singleshot, 5 Hz, 10 Hz or 20 Hz), as displayed in Figure 2 (A). For the other three emission bands available (10R, 9P and 9R), the problem is also present. A variation in the power measured was observed in all possible cases, emission bands and repetition rates available. The values could vary from 1 mJ up to 5 mJ for energy and 10 mW to 50 mW for power (repetition rate was 10 Hz in this measurement). The final acquisitions were recorded taking into account the improved procedure regarding the verification of a correspondence between the micrometer drive readings and wavelengths. It can be observed in Figure 2 (B) that the energy values for each repetition rates available were smoother and without significant deviations [5].

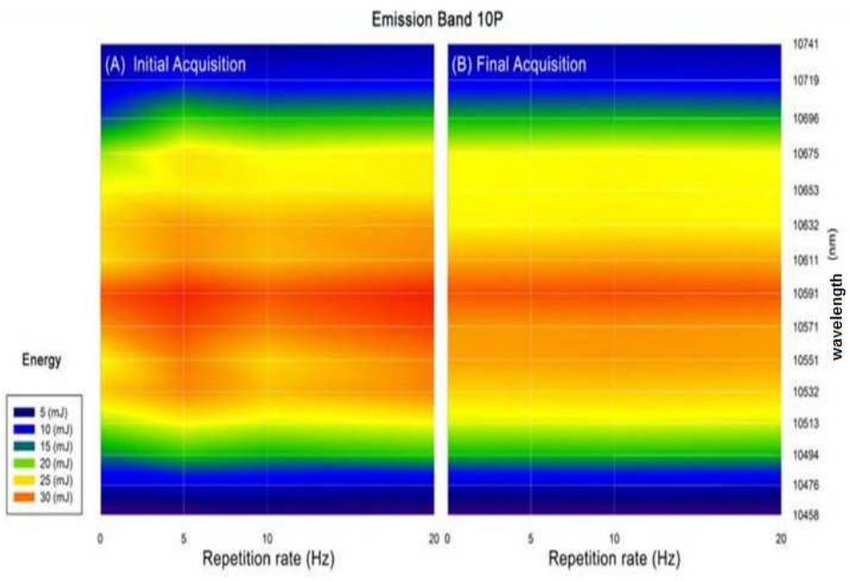

Fig. 2. Relationship between emission line, energy and repetition rates
(10P emission band-repetition rates single-shot, 5 Hz, 10 Hz and 20 Hz)

This has also been verified for the power values measured for the same repetition rates. The values still vary with the new procedure but in a much lower interval, between 0.5 mJ and 1 mJ for energy, and 5 mW and 10 mW for power values. The same improvement was verified for higher repetition rates up to 100 Hz. The confirmation could be observed not only for the 10P emission band (Figure 3), but also for the other three emission bands available (10R, 9P and 9R) [5].

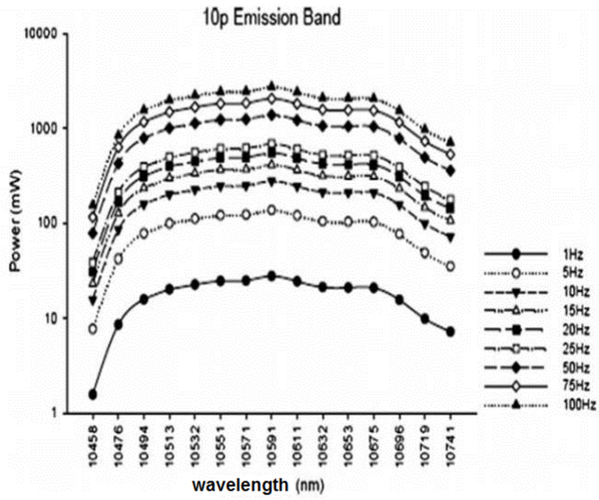

Fig. 3. Power versus repetition rate for 10P emission band.

Along this book chapter, several examples of CO_2 lasers applications to nanoscale science and nanotechnology, are explored and generally explained. These include examples in different topics, namely molecular photodynamics, tailored-size nanoparticles production, optical spectroscopy of nanopowders, infrared irradiation of nanostructures, desorption kinetics, photodynamic therapy, among others.

2. Laser spectroscopy and photodynamics

The combination of pulsed lasers, pulsed molecular beams and time-of-flight mass spectrometry represents a powerful technique for studying excitation, ionization and fragmentation of wanted molecules out of a large variety of different species present in a molecular beam [7]. The success of these two combined techniques is mainly due to the increase in the spectral resolution of absorption and fluorescence spectra by using collimated molecular beams with reduced transverse velocity components, and also to the fact that internal cooling of molecules during adiabatic expansion of supersonic beams compresses their population distribution into the lowest vibrational-rotational levels. This particular aspect greatly reduces the number of absorbing levels and results in a huge simplification of the absorption spectrum [7].

In addition, the low translational temperature achieved in supersonic beams allows the generation and observation of loosely bound van der Waals complexes and clusters. The collision-free conditions in molecular beams after their expansion into a vacuum chamber facilitates saturation of absorbing levels, since no collisions refill a level depleted by optical pumping. This makes Doppler-free saturation spectroscopy feasible even at low cw laser intensities [1].

The structure of molecular complexes in their electronic ground state can be obtained from direct infrared laser absorption spectroscopy in pulsed supersonic-slit jet expansions. This

allows one to follow the formation rate of clusters and complexes during the adiabatic expansion. Selective photodissociation of van der Waals clusters by infrared lasers could be used for isotope separation [1].

A typical example of a beam-gas collision is the process

$$Ca^*(^3P_J) + HCl \rightarrow CaCl(X;v'',J'') + H$$

The reaction with the ground state $Ca(^1S_0)$ is endothermic and this is why excited Ca atoms are required. When interrogating the centre of the reaction cell with a tuneable cw laser, Laser Induced Fluorescence (LIF) emission is observed on transitions in the CaCl(A-X) band system [2]. An example of a fraction of the related LIF excitation spectrum is shown in Figure 4.

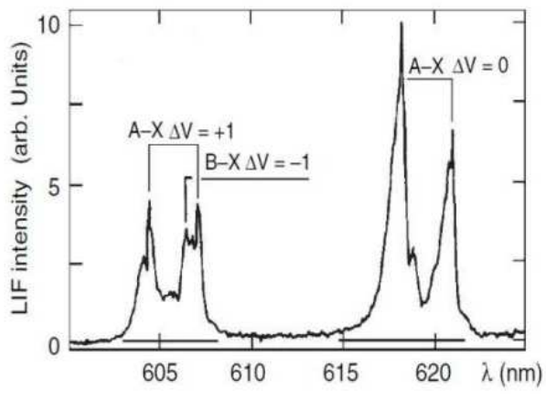

Fig. 4. LIF spectroscopy of the beam-gas reaction, revealing part of the rotational level population of the reaction product.

Important analytical applications are represented by measurements of the internal-state distribution of reaction products with LIF and spectroscopic investigations of collision-induced energy-transfer processes. The high output power of pulsed CO_2 lasers allows excitation of high vibrational levels by multiphoton absorption, which eventually may lead to the dissociation of the excited molecule. In some favorable cases the excited molecules or the dissociation fragments can even selectively react with other added components. Such selectively initiated chemical reactions can be induced by CO_2 lasers which are particularly advantageous due to their large electrical efficiency.

As an example, let us consider the synthesis of SF_5NF_2 by multiphoton absorption of CO_2 photons in a mixture of S_2F_{10} and N_2F_4, which proceeds according to the following scheme:

$$S_2F_{10} + nh\nu \rightarrow 2SF_5$$

$$N_2F_4 + nh\nu \rightarrow 2NF_2$$

$$SF_5 + NF_2 \rightarrow SF_5NF_2$$

This laser-driven reaction proceeds much more quickly than the conventional high-temperature synthesis without laser, even at the lower temperature of 350 K.

Another example of CO_2 laser-initiated reactions is the gas-phase telomerization of methyl-iodide CF_3I with C_2F_4, which represents an exothermic radical chain reaction

$$(CF_3I)^* + nC_2F_4 \rightarrow CF_3(C_2F_4)_nI \qquad (n = 1, 2, 3)$$

producing $CF_3(C_2F_4)_nI$ with low values of n. The CO_2 laser is in near resonance with the $\nu_2+\nu_3$ band of CF_3I. The quantum yield for this reaction increases with increasing pressure in the irradiated cell [2].

The infrared lasers have the advantage that the contribution of scattering losses to the total beam attenuation is much smaller than in the visible range. For measurements of very low concentrations, on the other hand, visible dye lasers may be more advantageous because of the larger absorption cross sections for electronic transitions and the higher detector sensitivity.

The applications of lasers to chemical reactions in gas phase are usually classified in two categories: laser induced chemical reactions and laser catalyzed chemical reactions. In the first ones, the laser supplies all the energy thermodinamically needed for the occurence of the reaction and they correspond typically to unimolecular processes (dissociation by multiphotonic absorption); in the second ones (typically bimolecular reactions) only a partial energy amount is supplied and then reaction proceeds by itself. The dissociation by multiphotonic absorption has seen a huge growth in the last decades [8] due to the availability of high power infrared lasers and important technological applications, like isotopic separation. As an example, since in SF_6 a mixture exists of $^{32}SF_6$ and $^{34}SF_6$, an infrared CO_2 laser with $\lambda = 10.61$ μm only gives rise to the excitation of vibrational states of $^{32}SF_6$ but not those of $^{34}SF_6$; thus, when the continuum of $^{32}SF_6$ vibrational states is reached after the absorption of 25 photons, only dissociation into $^{32}SF_5$ and F is produced. This dissociation is fast and corresponds to a statistical mechanism. On its turn, when the wavelength is tuned to 10.82 μm, the dissociation takes place in the $^{34}SF_6$ molecules.

The observation of dissociation phenomena in molecular beam apparatuses proves unequivocally that it is unimolecular and non-collisional, as it was shown through energetic and angular distributions of the SF_5 fragment formed in the dissociation of a SF_6 molecular beam, by a CO_2 laser pulse of 5 J/cm^3 [2]. Actually the results are consistent with RRKM unimolecular theory predictions. In this theory, it is assumed that energy is statistically distributed among the several available modes before dissociation takes place. This means that excitation energy is not localized in just one or a few modes, because in such cases, it will be not possible to reproduce with RRKM theory the above mentioned experimental results; in addition, the mean lifetime would be not about 10^{-8}s (as predicted by RRKM) but much smaller [2].

The dissociation of a polyatomic molecule by multiphotonic absorption is in fact a statistical process (i.e, non-selective), and allows to consider distinct types of selectivity with lasers, based on the existing relation between the different relaxation times which are involved in a vibrationally excited molecule:

$$\tau_{\text{intra v-v'}} << \tau_{\text{v-v'}} << \tau_{\text{v-T}}$$

where:

$\tau_{intra\ v\text{-}v'}$ - relaxation time for intramolecular vibrational energy transfer
$\tau_{v\text{-}v'}$ - relaxation time for vibrational energy transfer among distinct molecules
$\tau_{v\text{-}T}$ - relaxation time for vibration-translation transfer, i.e, the time needed to reach the complete thermal equilibrium

The first process can occur without collisions, but the other two are necesserelly collisional and therefore are pressure dependent. Considering v_{exc} as the vibrational excitation velocity of a molecule by multiphoton ionization (i.e, $1/v_{exc}$ will be the excitation time, which depends on radiation intensity and on the vibrational transition cross-section), a comparison of v_{exc} with the several excitation velocities, gives rise to four different situations:

- $v_{exc} >> 1/\tau_{intra\ v\text{-}v'}$; the excitation by absorption is faster than intramolecular relaxation, and so selective excitations are making possible; thus, a certain polyatomic molecule vibrational mode can reach a vibrational temperature higher than the other remaining modes.
- $1/\tau_{intra\ v\text{-}v'} >> v_{exc} >> 1/\tau_{v\text{-}v'}$; this is the more common molecular selectivity situation, where despite there is no vibrational equilibrium among the several molecules, intramolecular equilibrium exists for those molecules which interact with the infrared electromagnetic field.
- $1/\tau_{v\text{-}v'} >> v_{exc} >> 1/\tau_{v\text{-}T}$; vibrational equilibrium among all the molecules is guaranteed, but there is no relaxation for the translational modes which produce heating; in these conditions, photochemical vibrational experiments can be performed whenever the reactions have a characteristic time not longer than $\tau_{v\text{-}T}$ and a small energy barrier.
- $1/\tau_{v\text{-}T} >> v_{exc}$; the vibrational and translational temperatures of all molecules are equal due to the vibrational excitation relaxation in the molecular collisions, which heats the system up.

The excitation spectrum obtained by LIF of the CN fragment (produced by multiphoton absorption in the infrared with a high power CO_2 laser) of the gas $H_2C{=}CHCN$, shows clearly the rotational fine structure of the (0,0) band of the CN violet emission, which allows to conclude that the rotational distribution is statistical and characterized by a certain Boltzmann temperature, confirming that the excitation energy is statistically redistributed in the dissociation by multiphoton absorption [9].

The ability to energize a specific molecular bond and thereby promote a certain desired reaction pathway, has been a widely pursued goal, called mode-selective control in molecular physics. Actually, tunable infrared lasers are very convenient tools to divert a reaction from its dominant thermal pathway toward an envisaged possible product. However, the surplus of vibrational energy tends to be redistributed rapidly within a molecule. An initially excited, high-frequency localized mode can quickly de-excite by transferring its energy into combinations of lower frequency modes. In large molecules, in condensed phases, and at surfaces, huge numbers of low-frequency modes can accept energy, and energy randomization is very rapid (generally on the picosecond time scale or faster). This way, energy does not remain localized in a bond for a sufficiently long time to influence a chemical reaction. Therefore, the resulting chemistry is thermal rather than selective, which leads to the breaking of the weakest bond or to the reaction of the most reactive site. However, in small molecules with sparse vibrational modes, only a few or even

zero combinations of low-frequency modes can accept the energy, and so the lifetime of the initially excited mode may be sufficiently long to allow mode-selective chemistry. This was already demonstrated for the outcome of the gas-phase reaction of H atoms with singly deuterated water (HOD) that can be controlled through laser excitation of specific HOD vibrational modes [10] and it is also illustrated in Figure 5 for a molecular case where one can take profit of the C - Cl bond being stronger than C - Br one.

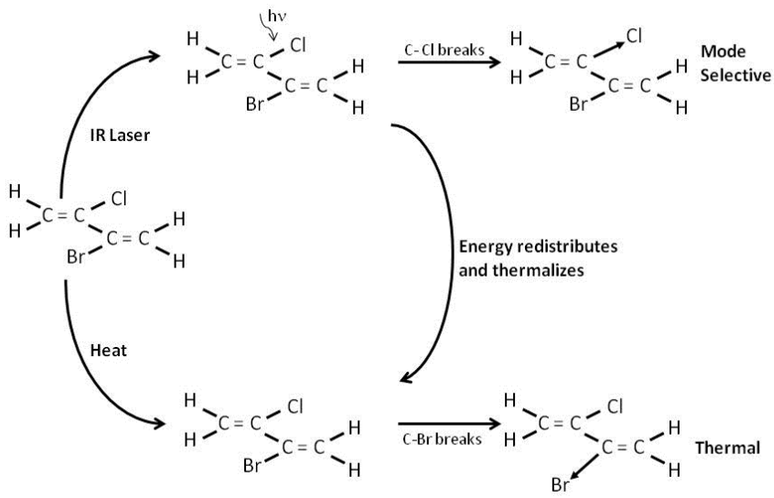

Fig. 5. LIF spectroscopy of the beam-gas reaction, revealing part of the rotational level population of the reaction product.

From the few attempts at IR mode-selective desorption of molecules from surfaces, that have been reported, perhaps the most successfull was the experimental findings of Liu et al [11], where the authors first created an absorbed layer of about 15% H atoms and 85% D atoms on an Si(111) surface. They then irradiated the surface with a free-electron laser tuned to the 4,8 μm Si-H stretching mode. They found that almost all desorbing atoms were in the form of H_2 and less than 5% of desorbing molecules were HD or D_2. This result rules out any local heating mechanism, which would produce a statistical mixture (2% H_2, 26% HD and 72% D_2). Largely as a result of the layer-molecular beam experiments of Y. T. Lee et al [12] the interpretation of the IR-MPD is now almost entirely clarified. The key to the understanding was the determination, under collision-free conditions, of the translational energy distribution of the photofragments as a function of laser intensity and, separately, laser fluence. It is found, indeed, that a suitable tailored statistical (RRKM) theory of unimolecular dissociation can explain most of the observations. All the evidence from these experiments suggests that mode selective molecular dissociation is only possible to achieve using a fast (ps) intense laser pulse.

Thermodynamic laws can be used to determine the equilibrium state of chemical reaction systems like the H_2/O_2 combustion ($2H_2 + O_2 = 2H_2O$). If chemical reactions are fast compared to all other physical processes (molecular diffusion, heat conduction and flow) thermodynamics alone allows the local description of even complex systems [13]. However, in most cases, chemistry occurs on time scales which are comparable with those of molecular transport. Thus, chemical kinetics information is required, e.g rate coefficients

k(T) of the individual elementary reactions which occur on the molecular level have to be known. For example, the above mentioned H_2/O_2 combustion reaction consists of 38 elementary reactions involving a variety of reactive intermediates like H, O atoms and OH radicals [14]. Laser pump-and-probe techniques, which combine pulsed laser photolysis for reactive species generation with time-resolved laser-induced fluorescence (LIF) detection for reaction products, have paved the way for detailed studies of the molecular dynamics of the elementary reactions [1,2].

The experimental possibilities for studying processes in technical combustion devices have expanded a lot in recent years as a result of the development of various pulsed high-power laser sources which provide high temporal, spectral and spatial resolution. Laser spectroscopic methods are important for non-intensive measurements in systems where complex chemical kinetics are coupled with transport processes. One of the key factors for improving the performance of many technical combustion devices is an optimum control of the ignition process. Optimized reproducible ignition ensures an efficient and safe operation. Actually, experimental studies on CO_2 laser-induced thermal ignition of CH_3OH/O_2 mixtures have been performed. In a quartz cell equipped with SrF_2 windows, CH_3OH/O_2 mixtures are ignited using a cw CO_2 laser in the pulsed mode. The coincidence of the 9P(12) CO_2 laser line in the (001)-(020) band with the R(12) CO stretch fundamental band of the methanol molecule at 9.6 μm allows controlled heating and ignition of the mixture. OH radicals formed during flame propagation were excited in the (v' = 3, v* = 0) vibrational band of the OH ($A^2\Sigma^+$ - $X^2\Pi$) transition around 248 nm using two tunable KrF excimer lasers (laser wavelength tunable in the range 247.9 - 248.9 nm with a bandwidth of typically 0.5 cm^{-1}). The time delay between the two excimer laser pulses is 100 ns, in order to separate the signals induced by them. The fluorescence is collected using achromatic UV lens. Reflection filters are used to spectrally isolate the (v' = 3, v'' = 2) fluorescence band of the OH radical for detection. Fluorescence is detected by gated image-intensified CCD cameras. Excitation of two different optical transitions starting from the N'' = 8 and N'' = 11 rotational levels of the OH ($X^2\Pi$ - v'' = 0) vibrational state, allowed the measurement of spatially corresponding LIF image pairs. Assuming a Boltzmann distribution for the population of the OH ($X^2\Pi$ - v'' = 0) rotational states, the ratio of the two OH fluorescence images can be converted into a OH temperature field [1,2].

Interest in infrared laser-induced chemical reactions centered on the quest for mode selectivity was sparked by work on laser isotope separation in the 1970s. In much of this work it is common to find a strongly increasing yield with fluence. However, it is much less common to find an increase with pressure. The most dramatic example of an increasing yield with pressure is the IR laser-induced reaction of isomerization of methyl isocyanid to acetonitrile. [15]. It was then demonstrated that absorption and dissociation can be significantly enhanced through collisions and such reaction exhibits a sharp threshold pressure above which nearly complete isomerization occurs in a single pulse. Thus, the laser-initiated isomerization of methyl isocyanide is an ideal reaction for examination of collision-induced energy transfer phenomena. For the fluence dependence experiments, the laser was operated on the P(20) 944.19 cm^{-1} transition of the 10.6-μm band. CaF_2 flats and KCl windows were used to attenuate the beam for the lower fluence data. For the wavelength data, the laser was operated on the P(6) through P(34) lines of the 10.6-pm band (corresponding to the maximum of the R through the maximum of the P branch of the ν_4(C-

N) stretch of methyl isocyanide) with an average energy per pulse of 1.05 J at the sample. Analysis for reaction was performed by monitoring the 2165 cm^{-1} ν_2(C=N) stretch with a grating spectrophotometer. To determine the relationship between fluence and threshold pressure, the fluence was kept constant while the pressure was varied so as to bracket the threshold. Then the process was repeated with a new fluence. The results indicate a linear variation of the fluence with the inverse of the pressure. Analysis of the fluence dependence of the threshold pressure indicates that the inverse of the threshold pressure is directly proportional to the average number of photons absorbed per molecule. This balance between incident fluence (or average number of photons absorbed) and threshold pressure can be understood in terms of the usual model of increasing yield with fluence. Hence, if the yield is increased owing to an increase in fluence, the threshold pressure should exhibit a concomitant decrease, as is observed. The multiphoton absorption spectrum as well as the wavelength dependence of the threshold pressure reflects the structure of the linear absorption spectrum [1].

Interest in using infrared laser radiation for studying charge transfer processes at surfaces relies on the possibility of exciting vibrational modes of adsorbate molecules. It is well-known that vibrational excitation is very important in promoting endoergic gas-phase chemical reactions, as well as in controlling chemical processes occurring in adsorbed layers. The use of IR lasers for initiating gas-surface reactions when the gas consists of polyatomic molecules allows us to put, at the gas-surface interface, a large amount of energy due to IR multiphoton absorption. As is known from gas-phase experiments, at rather moderate for IR $C0_2$ laser energy fluences of about 1 J/cm^2, it is possible to excite to high vibrationally excited states (up to energy levels E > 1 eV) practically all irradiated molecule. Therefore, in spite of a rather small value of $C0_2$ laser quantum (0.1-0.12 eV) and longer pulse duration (>100 ns), one can induce effective charge transfer.

The use of a pulsed TEA C02 laser allowed us to apply the time-of-flight (TOF) technique for the detection of ion signal and, as a result, to distinguish between molecular negative ions and electron emission. A TEA $C0_2$ laser line tunable in the range 9-11 μm was used for the excitation of molecules at the Ba surface. The laser beam was directed to the Ba surface perpendicular to the SF_6 beam direction via a ZnSe window in the HVC and a KBr window in the UHVC [16]. The negative molecular ion signal was shown to be very sensitive to the SF_6 molecular absorption (to the exciting $C0_2$ laser frequency). Thus, enhancement factors of 10 or 4 were found for 10P(20) versus 10R(20) and 10P(16) versus 10P(22) lines, respectively. This support the vibrational selectivity (vibrational enhancement) of the SF_6 + Ba gas-surface IR laser-photoinduced ionization process [16].

Regarding applications in cluster spectroscopy, some experiments have been performed, in particular infrared photodissociation by crossing a continuous supersonic molecular beam of small methanol clusters with the radiation of a pulsed CO_2 laser [17] . Subsequent scattering by a secondary He beam disperses the cluster beam and allows the off-axis detection of selected cluster species, undisturbed by ionizer fragmentation artifacts. In the region of the ν_8 C-O stretching vibration, the dependence of IR photon absorption on laser frequency and fluence is investigated as a function of cluster size [17]. The predissociation spectrum of the dimer shows two distinct peaks at 1026.5 and 1051.6 cm^{-1} which correspond to the excitation of the two non-equivalent monomers in the dimer. The trimer spectrum

features one single peak centered at 1042.2 cm^{-1}. This is consistent with a cyclic structure in which all three methanol molecules are equivalent. Higher cluster spectra are characterized by single peaks gradually blue-shifted with respect to the trimer line [17].

LIF detection is also used for various ultrasensitive techniques by probing reagents that are either autofluorescing or tagged with a fluorescent dye molecule. Applying different microscopic techniques with tight spatial and spectral filtering, various groups have directly visualized a variety of single fluorescent dye molecules (rhodamines and coumarins), dissolved in liquids by using coherent one- and two-photon excitation. Photophysical parameters and photobleaching play a crucial role for the accuracy of single-molecule detection by LIF and for the high sensitivity of fluorescence spectroscopy. Key properties for a fluorescent dye are its absorption coefficient, fluorescence- and photobleaching quantum yield. Photobleaching is a dynamic irreversible process in which fluorescent molecules undergo photoinduced chemical destruction upon absorption of light, thus losing their ability to fluoresce. Thus, for every absorption process there is a certain fixed probability ϕ_b of the molecule to be bleached. The probability P to survive n absorption cycles and become bleached in the $(n+1)^{th}$ cycle is given by:

$$P_{(\text{survival of n absorptions})} = (1- \phi_b)^n \phi_b$$

This corresponds to the geometric distribution, which is the discrete counterpart of the exponential distribution. Due to this exponential nature of the photodestruction process with the standard deviation $(1- \phi_b)/\phi_b$, the relative fluctuation of the number of detected photons due to a single molecule transit can be as high as 100% [18]. The mean number of survived absorption cycles μ is equal to the standard deviation:

$$\mu = (1- \phi_b)/\phi_b = 1/\phi_b$$

Photobleaching is the ultimate limit of fluorescence-based single-molecule spectroscopy, and the quantum yield of photobleaching is defined by the ratio:

ϕ_b = number of photobleached molecules/total number of absorbed molecules

Unfortunatelly, the total number of absorbed molecules cannot be measured directly and precisely under single-molecule-detection, making it impossible to determine ϕ_b. However, the above definition can be expressed in kinetic terms. If a dye solution is illuminated, it is possible to measure the number of irreversibly photobleached molecules as a decrease in the dye concentration c(t) with time t. Under appropriate conditions the rate of this decrease is proportional to c(t), and so photobleaching reaction can be treated as a quasi-unimolecular reaction:

$$dc(t)/dt = -k_b\, c(t) \quad \rightarrow \quad c(t) = c(0)\, e^{-k_b t}$$

The rate constant k_b is dependent on cw laser irradiance, and the study of this dependence can lead to the evaluation of ϕ_b. The photostability of many organic dyes in organic solvents is higher than in water.

Pursuing the goal of single-molecule spectroscopy where ultra-low concentrations of the fluorophore in water (< 10 pM) are used, we should focus on photoreactions occuring under these conditions. In single-molecule spectroscopy, photostability and fluorescence

saturation of the fluorophores impose limitations on the achievable fluorescence flow and the resulting signal-to-background ratio.

The rate constants for excitation from a state *i* to a state *f* are proportional to the irradiance *I* [W/cm^2] and to the absorption cross section $Q_{if}(\lambda)$ [cm^2] at a wavelength λ:

$$k_{Tif}(\lambda) = I\, Q_{if}(\lambda)\, \gamma$$

where = $\gamma/(hc)$, being *c* the velocity of light in vacuum and *h* the Planck constant.

Fluorescence saturation follows from the fact that a molecule cannot be in an electronically excited state and in the ground state at the same time; i.e. a single molecule can emit only a limited number of fluorescence photons in a certain time interval. Thus, the saturation characteristics of the fluorescent flows are determined by ground state depletion due to the finite excited state lifetimes of the S_1 and T_1 states (Figure 6).

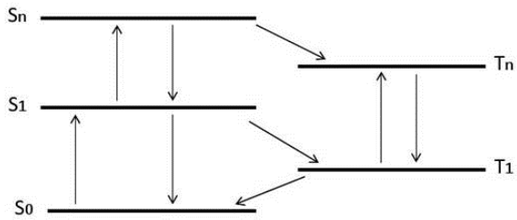

Fig. 6. Electronic Energy Diagram of a dye molecule with 5 electronic levels: S - singlet states; T - triplet states

The main reasons for using in life sciences near-infrared and infrared dyes as infrared fluorophores are threefold (although they photobleach more readily than dyes emitting in the visible):

- near-infrared dyes require excitation near IR which produces almost no auto-fluorescence from any endogenous components; hence, the sensitivity of detection, often limited by the auto-fluorescence background, is significantly improved.
- the laser wavelength also produce reduced scattering in the biological tissue, and thus increase both the penetration depth and the efficiency of collection of emission.
- available low-cost and compact NIR and IR diode lasers (e.g. 650 nm, 800 nm, 970 nm, etc...) can be used as excitation sources for these dyes.

Most of these dyes are cyanines, and they display a common problem which is their stability in biological fluids (composed mainly of water). They tend to aggregate, and so contribute to the quenching of emission. One method of preventing such aggregation is to isolate the dyes by encapsulation (in a nanobubble or a liposome) or to use chemical functionalization.

3. Nanoparticles and carbon nanotechnology

Given the importance of nanoscale particles in present technology, size distribution is a fundamental aspect as a quality control parameter. The production of nanoparticles using laser-induced gas-phase reactions techniques assures in general narrow size distributions contrarily to chemical techniques (such as precipitation or sol-gel processing) or to usual vapor-phase methods (furnace-heated vapor or arc-plasma), while the low reaction volume

and ability to maintain steep temperature gradients allows for precise control of the nucleation and growth rates favoring the formation of very fine and uniform powders. When reaction occurs in the gas phase, far from polluting walls very pure nano-scale materials may be prepared, and so conditions are created permitting the homogeneous nucleation of particles by condensation from a supersaturated vapor phase. In addition, the laser processing is cleaner.

Pulsed laser ablation of materials in aqueous solutions of surfactants can also lead in some cases to the formation of ultrafine particles as in the case of TiO_2 crystalline anatase 3 nm nanoparticles, using the third harmonic of a Nd:YAG laser (355 nm) operating at 10 Hz [19].

Laser-induced production of silicon nanoparticles has been mostly based on the global reaction

$$SiH_4\,(g) + nh\nu \rightarrow Si(s) + 2H_2\,(g)$$

Silane strongly absorbs in the ν_4 band at 10.5 μm resonant with the P(20) line of the $00^o1\text{-}10^o0$ transition at 944.19 cm^{-1} of the CO_2 laser [20]. Experiments have been performed in high vacuum with a pulsed TEA CO_2 laser at fluences that varied between 0.5 J/cm^2 and 150 J/cm^2 (using different converging focal distance infrared lenses). The shape and size of the nanoparticles is then examined by electron microscopy (SEM and TEM) and Atomic Force Microscopy (AFM), and their structure by X-ray diffraction [21,22]. Figure 7 schematically describes the experimental set-up for laser pyrolysis (chemical decomposition by heat in the absence of oxygen). Silane gas is laminarilly flowing through the center of the laser pyrolysis reactor, surrounded by another laminar flow of helium. The focalized laser pulse (Δt = 100 ns, I = 30-40 mJ/pulse) decompose silane into silicon and hydrogen atoms which then recombine to form molecular hydrogen. Since a nozzle is placed close to the reaction zone, the silicon atoms and small silicon clusters are extracted in the majority helium supersonic expansion (like an ultra-fast cooler at a rate of 10^9 Ks^{-1}), giving rise by condensation to larger clusters and nanoparticles. Their formation is processing in bursts of some nanoseconds, according to the laser pulses characteristics. The nanoparticles size selection is assured by a synchronized chopper with the laser pulses, and the size distribution is measured in-situ by time-of-flight mass spectrometry (TOFMS). It is also possible to deposit these silicon nanocrystals on a removable target mica substrate [21,22].

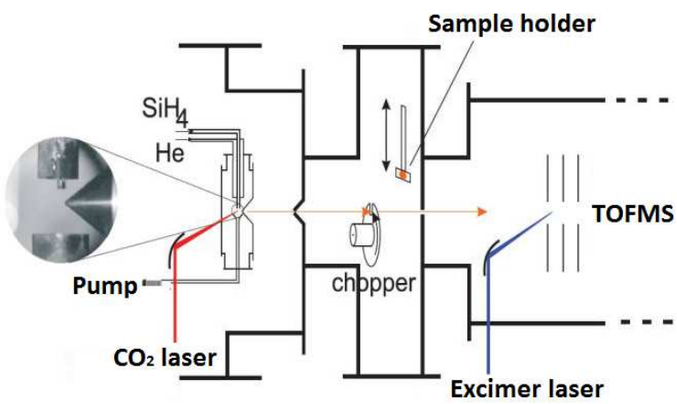

Fig. 7. Laser pirolysis set-up for size-selected nanoparticles production [21,22].

The kinetic energy of the clusters is small (less than 0.4 eV per atom for 4 nm size particles, which corresponds to 10% of the bonding energy) and so a Low Energy Cluster Beam Deposition (LECBD) is taking place, without changing the cluster properties in gas phase. Due to the geometry of the system, a distribution of nanoparticle sizes also appears on the substrate, and it can be guaranteed that all the sizes correspond to the same air exposition history. By varying some experimental parameters (pressure, flow, laser power, delay between laser pulse and chopper slit) it is possible to control the size distribution of the silicon nanoparticles deposited onto the substrate, for ultramicroscopic analysis (Figure 8).

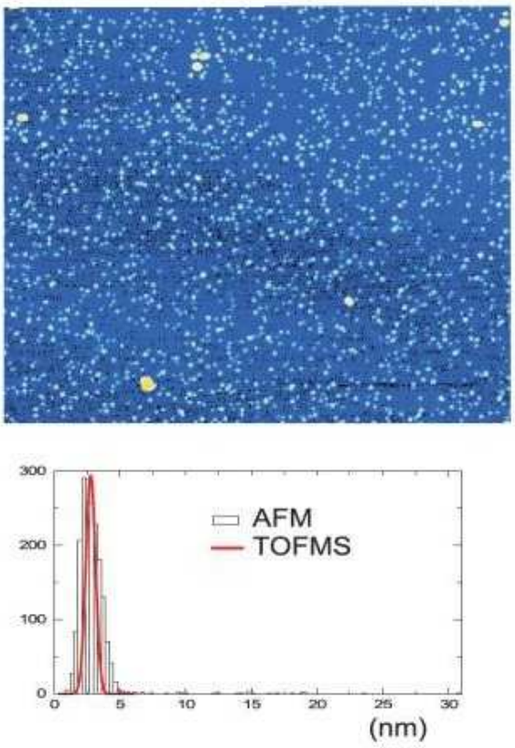

Fig. 8. AFM image of size-selected silicon nanoparticles together with their size distributions measured by TOFMS and AFM[21,22].

The advantage of using a TEA CO_2 laser in the pyrolysis becomes clear for the fine tuning wavelength adjust, in order to optimize the production process of several other types of nanoparticles [22].

Several synthesis reactors geometries based on the vaporization of a target (graphite/metal catalyst pellet) inside a oven at a fixed temperature (above 1000 K) by continuous CO_2 laser beam (λ = 10.6 μm) have been developed to produce several types of carbon nanotubes. The laser power can be varied from 100 W to 1600 W and the temperature of the target is measured with an optical pyrometer. In general a inert gas flow carries away the solid particles formed in the laser ablation process which are then collected on a filter [23].

A typical mid-IR to near-IR absorbance spectrum taken on uniformly dispersed, purified CNTs (grown by CVD-mostly MWNT) at room temperature is displayed in Figure 9 [24]. In the measured IR absorbance spectrum, a prime intensity peak is seen at 1584 cm^{-1}. This is an

IR-active, graphite-like E_{1u} mode (also known as the *G* band) originating from the sp_2-hybridized carbon. The absorbance peak at 1200 cm^{-1}, is a disorder-induced one phonon absorbance band (D band-from the sp_3-hybridized carbon), which has been also observed in neutron irradiated diamonds [24]. This lattice mode arises from the disruption of the translational symmetry of the diamond lattice. In general, the presence of CH_x groups (evidenced in the IR active bands in the range of 3000 cm^{-1}) and non-conjugated carboxylic carbonyl groups (peak around 1725 cm^{-1}) can benefit a number of bio-sensing applications by offering a simple route to nanotube functionalization [25].

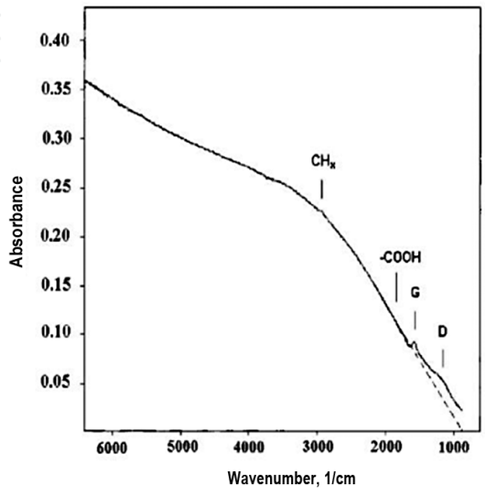

Fig. 9. Typical infrared absorbance spectrum obtained on 60 nm multiwall carbon nanotubes [25]

Production of single-wall carbon nanotubes (SWNT) by the laser-ablation technique using graphite, pitch and coke as carbonaceous feedstock materials has been reported [26]. This has been done with a 250W continuous-wave CO_2-laser at a wavelength of 10.6 μm and varying the nature and the concentration of the metal catalyst, the type and pressure of the buffer-gas as well as the laser conditions. The amount of SWNT material obtained is much higher when using graphite as a precursor than in the case of coke and carbonaceous feedstock [26].

Laser-assisted chemical vapour deposition (LCVD) for the formation and growth of carbon nanotubes has also been performed using a medium-power continuous-wave CO_2 laser to irradiate a sensitized mixture of $Fe(CO)_5$ vapour and

acetylene and to simultaneously heat a silicon substrate on which the carbon nanotubes were grown [27]. Electron microscopy (TEM and HRTEM) as well as atomic force microscopy (AFM) were used to analyze the as-grown films and samples specially prepared on TEM grids and AFM substrates. Carbon nanotubes with different structures (straight, curved and even branched), including single- and multi-walled nanotubes were observed. Some nanotubes were found to be partially filled with a solid material (probably metallic iron) that seems to catalyze the nanotube growth [27].

Using a CO_2 laser perpendicularly directed onto a silicon substrate, sensitized mixtures of iron pentacarbonyl vapour and acetylene were pyrolyzed in a flow reactor. The method involves the heating of both the gas phase and the substrate by IR radiation. The carbon

nanotubes were formed via the catalyzing action of the fine iron particles produced in the same experiment by the decomposition of the organometallic precursor molecules [27]. The reactant gas, a mixture of iron pentacarbonyl vapour ($Fe(CO)_5$), ethylene (C_2H_4) and acetylene (C_2H_2), is admitted to the reaction cell through a rectangular nozzle, creating a gas flow close and parallel to the Si substrate and being pumped from the opposite side. The flow of ethylene is directed through a bubbler containing liquid iron pentacarbonyl at room temperature (and 27 Torr vapour pressure). Thus, the ethylene serves as carrier gas for the iron pentacarbonyl. The third gas, acetylene, is supplied by an extra line. Before entering the flow reactor, the gases are mixed in a small mixing vessel. The iron nanoparticles, needed to catalyze the formation of carbon nanotubes from carbon-containing precursors, are obtained by decomposing $Fe(CO)_5$ during the laser-induced reaction. Ethylene gas, introduced into the gaseous atmosphere, serves also as a sensitizer activating the laser reaction and speeding up the $Fe(CO)_5$ dissociation. C_2H_4 has a resonant absorption at the CO_2 laser emission wavelength (10.6 μm) and is characterized by a rather high dissociation energy. Under the present conditions, C_2H_4 is only expected to collisionally exchange its internal energy with the other precursor molecules that do not absorb the CO_2 laser radiation, thus heating the entire gas mixture [27].

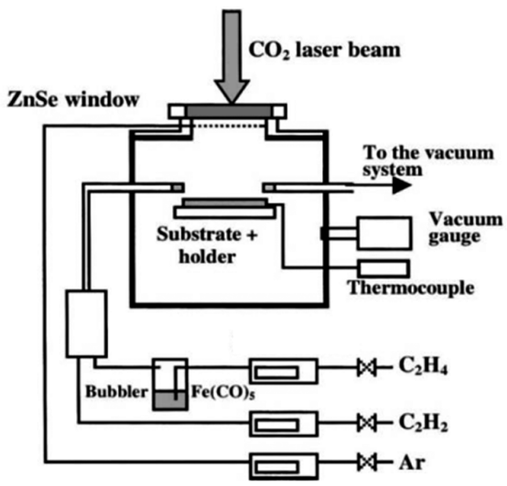

Fig. 10. Experimental set-up for the deposition of carbon nanotubes by LCVD
Adapted from [27]

The pressure inside the reaction chamber was keptat a constant value of 150 Torr. A flow of argon (500 sccm) was used to avoid contamination of the ZnSe entrance window during irradiation. At the heated surface and interface, iron pentacarbonyl is the first molecule to undergo dissociation, which can proceed until bare iron is obtained. Carbon nanotubes with straight, curved or even branched structures have been identified by ultramicroscopy. While some nanotubes were hollow, many of them were found to be partially or totally filled with nanoparticles most probably being metallic iron [27].

Films of vertically aligned MWCNTs of extremely high packing density were produced by this technique under very clean hydrocarbon supply conditions. Using an open-air pyrolitic LCVD system in which the role of gas-phase reactions are minimized, the growth of highly oriented and aligned single- and multiwall carbon nanotubes have been reported [28]. The

LCVD technique in general has several prominent advantages including high deposition rates that are favorable for scale-up production of CNTs. In contrast to the standard LCVD system, in which the in situ thermal decarbonylation of $Fe(CO)_5$ is used for obtaining Fe nanoparticles C-LCVD employs the catalytic activity of pre-deposited metal-based nanoparticles. For a better control of CNT growth conditions, it proved to be advantageous to carry out separately the catalyst deposition and carbon nanotube growth. Thus, as a main advantage, C-LCVD allows *ex-situ* prepared metal-based particles with the desired properties and dispersion degree to provide the nucleation conditions for the growth of CNTs [28]. The temperature is measured with a thermocouple positioned behind the substrate. Since the temperature of the area which is irradiated by the laser is expected to be considerably higher than the average temperature of the substrate holder, the temperature inside the laser spot is measured optically with a pyrometer. Under a total gas pressure of about 80 mbar, the temperature in the laser spot, measured with the pyrometer could reach values between 800 and 900 C, while the thermocouple indicates values that are about 100 C lower. Mainly depending on the ethylene concentration, nanotube mean diameters between 10 and 60 nm were found. By increasing ethylene precursor flow rate, not only larger mean diameters of the CNTs were found but also the distribution of the CNT diameters became broader [28].

Cementite (Fe_3C) is of great technological importance for the mechanical properties of steels and iron alloys and for its role as catalyst to produce various hydrocarbons (including olefins, from CO_2 and H_2) and preferred catalysts for carbon fibers, nanotubes and nanoparticles due to their low nanometric mean sizes and narrow size distributions. Pure Fe_3C nanomaterials have also been obtained by the pyrolysis of methyl methacrylate monomer, ethylene (as sensitizer), and iron pentacarbonyl (vapors) in a suitable range of laser intensities (by irradiating the same reactive mixture with a lower intensity radiation, the chemical content of the produced nanoparticles shifts towards mixtures of iron and iron oxides). Such nanopowders exhibited core (Fe_3C)–shell polymer-based morphologies and their magnetic properties are likely to display high values for the saturation magnetization.

Semiconductor photocatalysts have been used in different applications, and the combination of high photocatalytic activity, high stability and the benefit of environmental friendliness makes titanium dioxide the material of choice for such applications. In order to enhance the performance of this material for industrial purposes, coupling of TiO_2 with other semiconductors and immobilization of TiO_2 on porous materials have been studied as means for improving its photocatalytic activity. Nanocomposites of TiO_2 and multi-walled carbon nanotubes were prepared and deposited by sol–gel spin coating on borosilicate substrates and sintered in air at 300 ºC. Further irradiation of the films with different CO_2 laser intensities was carried out in order to crystallize TiO_2 in the anatase form while preserving the MWNT's structure. The laser irradiation changed the crystal structure of the coatings and also affected the wettability and photocatalytic activity of the films. The anatase phase was only observed when a minimum laser intensity of 12.5 W/m^2 was used [29]. The contact angle decreased with the enhancement of the laser intensity. The photocatalytic activity of the films was determined from the degradation of a stearic acid layer deposited on the films. It was observed that the addition of carbon nanotubes themselves increases the photocatalytic activity of TiO_2 films. This efficiency is

even improved when high CO_2 laser intensities are used during the sintering of the coatings [29].

The high aspect ratio combined with high mechanical and chemical stability of carbon nanotubes could help in enhancing the photocatalytic activity of TiO_2. Nanocomposites of TiO_2/CNTs were prepared by the addition of $-NH_2$ functionalized, 10 nm outer diameter MWNTs to the TiO_2-based sol, in a concentration of 3 mg/ml. After a fine dispersion of the nanotubes was achieved using a high shear processor, the sol was deposited on borosilicate glass substrates by a spin coating technique (2000 rpm, 10 s) [29].

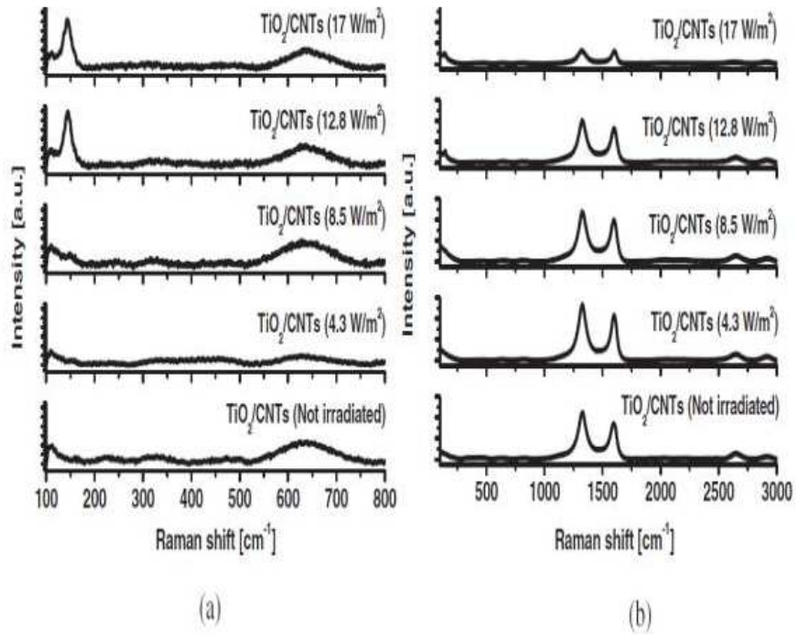

Fig. 11. Raman spectra in the ranges (a) 100-800 and (b) 300-3000 cm^{-1} of TiO_2/MWNT coatings not irradiated and irradiated with different CO_2 laser intensities [29]

Raman spectra of TiO_2/MWNT coatings not irradiated and irradiated with different CO_2 laser intensities are shown in Figure 11. Non-irradiated films sintered in air at 300°C have shown no Raman bands, as is clear from Figure 11 (a). Higher sintering temperatures were applied to the coatings inorder to obtain anatase TiO_2 phase structure, but oxidation of the MWNTs took place, limiting the study of the composites. Therefore, CO_2 laser irradiation was applied to the coatings with different density outputs as an alternative sintering process. This process is very fast, and because it is pulsed (highly spatially limited heated zone), it has not damaged the CNT's structure. Films irradiated with lasers of intensity lower than 12.8 Wm^{-2} have shown similar results to non-irradiated coatings in the range 100–1000 cm^{-1} [29]. However, a sharp and intense Raman band at 144 cm^{-1} corresponding to anatase TiO_2 phase was observed when such minimum laser intensity was applied during the sintering of the coatings, suggesting that the local temperature obtained using 12.8 Wm^{-2} is sufficient to crystallize the coating. Figure 11 (b) shows D and G bands corresponding to the presence of MWNTs at 1319–1328 and 1592–1601 cm^{-1}, respectively. The D band corresponds to defects present in carbonaceous materials. The addition of CNTs to the TiO_2

matrix improved the photocatalytic activity of TiO_2 coatings, as has been demonstrated by the degradation of a stearic acid layer deposited on the films [29]. In addition, higher CO_2 laser intensities during the sintering implies enhanced photocatalytic activity of the nanocomposites.

Laser Induced Breakdown Spectroscopy (LIBS) and Laser Induced Incandescence (LII) are two suitable techniques for analyzing small particles. In LII a pulsed laser rapidly heats the particles and by monitoring the rate of decay of the resulting incandescent radiation, one can extract particle size information, as the rate is related to the size of the particle. In order to get information on the particles chemical composition LIBS must be used instead. With it, the pulsed laser is tightly focused on the sample to induce a breakdown (microspark) of the material, and so by monitoring the emission of light from this plasma one can gather information about chemical compositions. Sensor technology is now able to capture light between 200 and 940 nm, a region where all elements emit. Since LIBS data is generated in real-time (response time of 1 second or less), one keep track of rapid changes in the composition of the particles during the actual production run. LIBS is very sensitive, having a resolution in the femtogram region and capable of detecting as few as 100 particles/cm^3.

Irradiating the surface of a solid with a laser, material can be ablated in a controlled way by optimizing intensity and pulse duration of the laser (laser ablation). Depending on the laser wavelength, the ablation is dominated by thermal evaporation (using a CO_2 laser) or photochemical processes (using an excimer laser). Laser-spectroscopic diagnostics can distinguish between the two processes. Excitation spectroscopy or resonant two-photon ionization of the sputtered atoms, molecules, clusters, nanoparticles or even microparticles allows their identification (Figure 12).

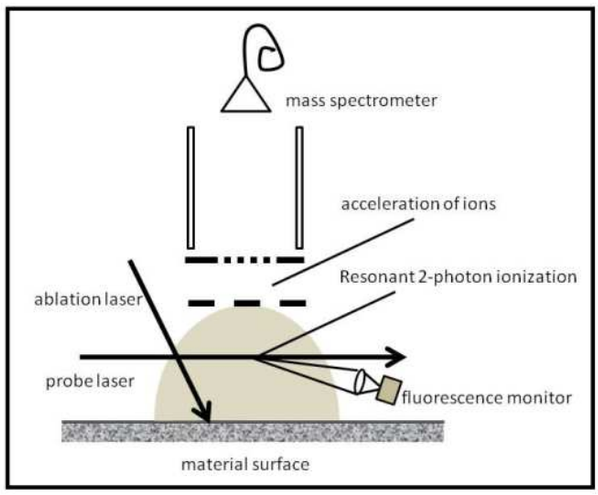

Fig. 12. Laser ablation from a surface

In addition, the velocity distribution of particles emitted from the surface can be obtained from the Doppler shifts and broadning of the absorption lines, and their internal energy distribution from the intensity ratios of different vibrational-rotational transitions. With a pulsed ablation laser, the measured time delay between ablation pulses and probe laser

pulses allows the determination of the velocity distribution. Resonant two-photon ionization in combination with a TOFMS gives the mass spectrum. It is common to observe a broad mass range of clusters. The question is whether these clusters were emitted from the solid or whether they were formed by collisions in the evaporated cloud just after emission. Measurements of the vibrational energy distributions can give an answer. If the mean vibrational energy is much higher than the temperature of the solid, the molecules were formed in the gas phase, where an insufficient number of collisions cannot fully transfer the internal energy of molecules formed by recombination of sputtered atoms into kinetic energy.

Whereas laser ablation of graphite yields thermalized C_2 molecules with a rotational-vibrational energy distribution following a Boltzmann distribution at the temperature T of the solid, ablation of electrical insulators, such as AlO, produces AlO molecules with a large kinetic energy (≈1 eV), but a "rotational temperature" of only 500 K.

4. Technological applications

Photodynamic therapy (PDT) is used clinically to treat a wide range of medical conditions, including malignant cancers, and is recognised as a treatment strategy which is both minimally invasive and minimally toxic. Photosensitization is a process of transferring the energy of absorbed light. After absorption, the energy is transferred to the (chosen) reactants. This is part of the work of photochemistry in general. In particular this process is commonly employed where reactions require light sources of certain wavelengths that are not readily available. For example, mercury absorbs radiation at 1849 and 2537 angstroms, and the source is often high-intensity mercury lamps. It is a commonly used sensitizer. When mercury vapor is mixed with ethylene, and the compound is irradiated with a mercury lamp, this results in the photodecomposition of ethylene to acetylene. This occurs on absorption of light to yield excited state mercury atoms, which are able to transfer this energy to the ethylene molecules, and are in turn deactivated to their initial energy state.

In order to achieve the selective destruction of the target biological area using PDT while leaving normal tissues untouched, the photosensitizer can be applied locally to the target area. For instance, in the treatment of skin conditions, including acne, psoriasis, and also skin cancers, the photosensitizer can be locally excited by a light source. In the local treatment of internal tissues and cancers, after photosensitizers have been administered intravenously, light can be delivered to the target area using endoscopes and fiber optic catheters. Compared to normal tissues, most types of cancers are especially active in both the uptake and accumulation of photosensitizers agents, which makes cancers especially vulnerable to PDT. Since photosensitizers can also have a high affinity for vascular endothelial cells, PDT can be targetted to the blood carrying vasculature that supplies nutrients to tumours, increasing further the destruction of tumours.

The optimal spectral window for biological tissue penetration of irradiation is around 800 nm to 1 μm. The use of CO_2 laser relies on water (the largest constituent of most biological tissues) absorbing strongly at 10.6 μm; this strong absorption leads to a shorter optical penetration depth (≈13 μm), limiting its use to extremely thin tissues. A patient would be given a photo sensitive drug (photofrin) containing cancer killing substances which are

absorbed by cancer cells. During the surgery, the light beam is positioned at the tumor site, which then activates the drug that kills the cancer cells, thus photodynamic therapy.

A sensitizer in chemoluminescence is a chemical compound, capable of light emission after it has received energy from a molecule, which became excited previously in the chemical reaction. A good example is when an alkaline solution of sodium hypochlorite and a concentrated solution of hydrogen peroxide are mixed, a reaction occurs:

$$ClO^-(aq) + H_2O_2(aq) \rightarrow O_2^*(g) + H^+(aq) + Cl^-(aq) + OH^-(aq)$$

$O_2^*$is excited oxygen - meaning, one or more electrons in the O_2 molecule have been promoted to higher-energy molecular orbitals. Hence, oxygen produced by this chemical reaction somehow 'absorbed' the energy released by the reaction and became excited. This energy state is unstable, therefore it will return to the ground state by lowering its energy. It can do that in more than one way:

- it can react further, without any light emission
- it can lose energy without emission, for example, giving off heat to the surroundings or transferring energy to another molecule
- it can emit light

New types of photosensitizers used in photodynamic therapy, which are based on photon upconverting nanoparticles, have been developed. Such photosensitizers are excitable with infrared irradiation, which has several times larger tissue penetration depth than the currently available ones. Photon upconverting materials convert lower-energy light to higher-energy light through excitation with multiple photons. For instance, such materials would adsorb infrared irradiation and emit visible light to further excite the photosensitizing molecules. Photon upconverting nanoparticles (PUNPs) play here a crucial role. They can be first coated with a porous, thin layer of silica through sol-gel reaction. During the coating process, photosensitizing molecules with high absorbance in the spectral window matching the emission of the PUNPs are doped, so that the resulting silica layer contains a certain amount of these photosensitizing molecules. Finally, an antibody, specific to antigens expressed on the target cell surface, is covalently attached to the silica-coated nanoparticles. When the thus-prepared nanoparticles are irradiated by infrared light, emission from the PUNPs will be absorbed by the photosensitizing molecules coated on their surfaces. Subsequently, excited photosensitizing molecules will interact with surrounding groundstate molecular oxygen, generating singlet oxygen, leading to oxidative damage of the neighboring cells to which the nanoparticles are attached via specific antigen-antibody binding.

PUNPs made from $NaYF_4:Yb^{3+},Er^{3+}$ have been recognized as one of the most efficient photon upconverting phosphors [30].

When excited by an infrared (974 nm) source, strong visible bands appear around 537 nm and 635 nm. Merocyanine 540 (M-540) is used as photosensitizing molecule, and doped into the silica layer during the coating process. M-540 is a molecule that can produce singlet oxygen and other reactive oxygen species, and has been used before in photodynamic therapy as a photosensitizer with a visible light source. Both the emission spectrum of $NaYF_4:Yb^{3+},Er^{3+}$ nanoparticles and the absorption spectrum of M-540 show a good overlap

between the nanoparticles' emission and M-540's absorption [30]. The photon upconverting property of the nanoparticles was not affected by the silica coating, as confirmed by their photoluminescence spectrum. The presence of M-540 in the silica coating could be readily confirmed by the change in color of the nanoparticles, to slightly yellowish.

Photosensitizers drugs, should ideally be specific to the target, highly effective in producing reactive oxygen species (ROS) when exposed to appropriate illumination, and excitable by a wavelength close to the near-infrared region (800 nm to 1 μm),where tissue penetration of the illumination is at a maximum.

Regarding the last desired feature, single photons with infrared wavelengths are usually too weak energetically to generate reactive oxygen species ($^1O_2$). Thus, multiphoton excitation would be needed for infrared light to be used as illumination source. It has been reported the synthesis and characterization of a type of nanomaterial capable of generating $^1O_2$ under continuous wave infrared excitation, based on photon upconverting nanoparticles (PUNPs). The results demonstrate that such nanoparticles have great potential for becoming a new type of versatile PDT drugs for photodynamic therapy [31]. Although photon upconverting materials do not directly produce ROS, one utilizes the fact that they adsorb infrared photons and emit visible ones to further excite the photosensitizing molecules, thus indirectly causing the photosensitizing molecules to generate $^1O_2$ under infrared excitation. The design and synthesis of the PUNP-based photosensitizers follow a schema depicted in Figure 13.

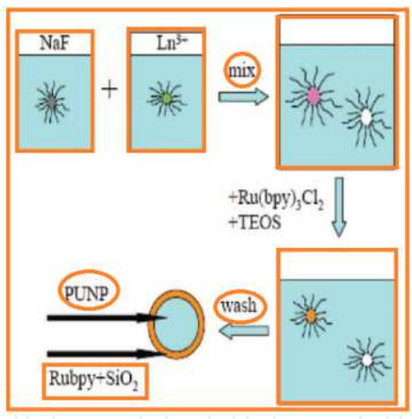

Fig. 13. PUNP-based photosensitizer preparation.

The core is a $NaYF_4$:Yb^{3+},Tm^{3+} nanoparticle, a photon upconverting material capable of emitting blue light (≈ 477 nm) upon excitation by an infrared light source (≈ 975 nm). The nanoparticle was then coated by a thin layer of tris(bipyridine)ruthenium(II)-doped silica which generates $^1O_2$. The $NaYF_4$:Yb^{3+},Tm^{3+} nanoparticles were synthesized by a microemulsion method [31].

The photoluminescence spectra of the $NaYF_4$:Yb^{3+},Tm^{3+} nanoparticles before and after beingcoated with Ru(bpy)3-doped silica, under 975 nm excitation, are shown in Figure 14.

One of the most sensitive methods to detect volatile compounds released by the plants is laser photoacoustic spectroscopy (LPAS), which allows the identification of many molecules

signaling plant defence mechanisms [32]. The technique is based on the photoacoustic effect, i.e. the generation of acoustic waves as a consequence of light absorption. The absorption of photons of a suitable wavelength and energy by the gas molecules excites them to a higher ro-vibrational state. The absorbed energy is subsequently transferred by intermolecular collisions to translational energy, and thereby to heat. When a gas sample is collected in a closed cell, the heating of the gas molecules will increase the cell pressure. Hence, by modulating the light intensity pressure variations are produced that generate a sound wave, which can be detected with a sensitive microphone. A schematic view of a typical LPAS experimental system for the detection of volatile molecules is shown in Figure 15.

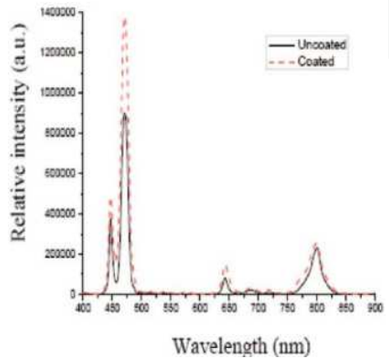

Fig. 14. Photoluminescence spectra of $NaYF_4$:Yb^{3+},Tm^{3+}nanoparticles before and after being coated with $Ru(bpy)_3$-doped silica [31]

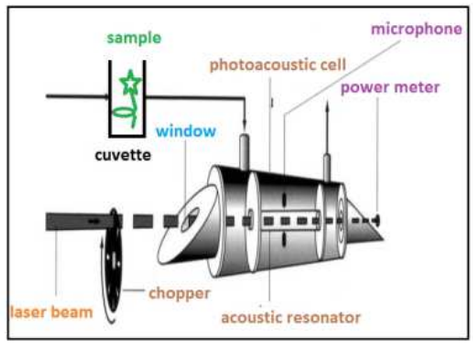

Fig. 15. Schematic view of a LPAS set-up for the detection of volatile molecule emission from plants.

The photoacoustic signal depends on the number of absorbing molecules present in the gas, the absorption strength of the molecules at a specific light frequency, and the intensity of the light. Then, for trace gas detection, the light source should have a narrow bandwidth and be tuneable (in order to match the specific molecular absorption feature), and it should have a high intensity to ensure a good signal-to-noise ratio. Since the absorption processes of interest involve ro-vibrational transitions, it is normally necessary to work in the IR region. In this spectral range each molecule has its own *fingerprint* absorption spectrum,whose strength can vary rapidly over a short wavelength interval. Specifically, the preferred range for spectroscopic applications lies in the range 3–20 μm. Specifically, CO_2 and CO lasers serve as the most frequently used light sources for photoacoustic detection of gases because

they provide relatively high CW powers, typically up to 100 W and 20 W respectively, over this wavelength region. LPAS shows a large versatility of applications not only in plant science, but also in other fields, e.g. in environmental chemistry [33]. It has been shown to be a reliable method for the detection of ethylene in several plant physiological processes at parts per trillion concentration levels (e.g. from a cherry tomato under different conditions) [34].

One of the major analytical problems with fruit and vegetable samples is the detection and identification of non-volatile organic compounds present in low concentration levels, as happens for most of the phytoalexins produced by plants. Mass spectrometry is widely used in the analysis of such compounds, providing exact mass identification. However, the difficulty with their unequivocal identification and quantitative detection lies in their volatilization into the gas phase prior to injection into the analyser. This constitutes particular problems for thermally labile samples, as they rapidly decompose upon heating. To circumvent this difficulty a wide range of techniques have been applied for non-volatile compound analysis, including LD (Laser Desorption). Recently, LD methods have been developed in which the volatilization and ionization steps are separated, providing higher sample sensitivity. In particular, REMPI-TOFMS is considered to be one of the most powerful methods for trace component analysis in complex matrices [2]. The high selectivity of REMPI-TOFMS stems from the combination of the mass-selective detection with the resonant ionization process, i.e. the ionization is achieved by absorption of two or more laser photons through a resonant, intermediate state. This condition provides a second selectivity to the technique, namely laser wavelength-selective ionization. In addition, it shows an easy control of the molecular fragmentation by the laser intensity and the possibility of simultaneous analysis of different components present in a matrix.

As an example, it is possible to perform fast and direct analysis of non-volatile compounds in fruit and vegetables, particularly *trans*-resveratrol in grapes and vine leaves. The method is based on the combination of LD followed by REMPI and TOFMS detection, often identified by its sum of acronyms, i.e. LD-REMPI-TOFMS [35]. *Trans*-Resveratrol is an antioxidant compound naturally produced in a huge number of plants, including grapes. Analysis of *trans*-resveratrol is generally carried out by high-performance liquid chromatography. Its analysis in grapes and wines requires the use of pre-concentration prior to analysis and/or multi-solvent extraction techniques, due to the complexity of the matrices and to the low concentration of the analyte. The extraction methods generally employed are liquid extraction with organic solvents or solid-phase extraction. It is generally accepted that the sample preparation is the limiting step in *trans*-resveratrol analysis, not only because of the need for costly and time-consuming operations, but also because of the error sources introduced during this operation. These error sources can largely be overcome when applying the method of LD-REMPI-TOFMS. The experimental set-up used in this analysis method basically consists of two independent high vacuum chambers; the first chamber is used for both laser desorption and laser post-ionization of the samples, and the second chamber for TOFMS [2].

Some other relevant technological applications of infrared lasers will be generally described here in the following paragraphs.

Katzir was the first researcher to apply the carbon dioxide laser, coupled to optical fibers made from silver halide, for wound closure under a tight temperature control. The fibers

deliver the laser's energy to heat the bonded cut and are used for controlling the temperature. They also make it possible to bond tissues inside the body. Sutures or stitches are not water tight, and blood or urine can pass through cuts, causing severe infection. Laser-bonded tissues heal faster, with less scarring. Even using today's microsurgery techniques, the treated wounds are open to infection, and the patient is inevitably left with permanent and unsightly scars. The near-infrared light is just the right wavelength to excite vibrations in chemical bonds in the water molecules (via first-overtone excitation in the OH-stretch manifold); the vibrations quickly turn into heat.

Keeping the heat from the laser at exactly the right temperature for optimal wound healing, allows surgeons to seal cuts both on our skin and inside our bodies with less scarring, and less exposure to infection. When the laser begins to overheat and risks burning the tissue, the device reduces laser power, and if the temperature is too low to complete a closure, laser power is increased appropriately.

There is also an enormous potential of a CO_2-laser system for rapidly producing polymer microfluidic structures. The common polymer poly (methyl methacrylate) (PMMA) absorbs IR light in the 2.8–25 μm wavelength band, so CO_2 lasers have been used in recent years for fabricating microfluidic devices from it, with channel widths of a few hundred micrometers. The narrowest produced channel was 85 μm wide. A solvent-assisted thermal bonding method proved to be the most time-efficient one. These systems provide a cost effective alternative to UV-laser systems and they are especially useful in microfluidic prototyping due to the very short cycle time of production.

Furthermore, surface heat treatment in glasses and ceramics, using CO_2 lasers, has drawn the attention to several technological applications, such as lab-on-a-chip devices, diffraction gratings and microlenses. Microlens fabrication on a glass surface has been studied mainly due to its importance in optical devices, as fiber coupling and CCD signal enhancement. Using microlens arrays, recorded on the glass surface, can enable the bidimensional codification for product identification. This would allow the production of codes without any residues (like the fine powder generated by laser ablation) and resistance to an aggressive environment, such as sterilization processes. Microlens arrays can be fabricated using a continuous wave CO_2 laser, focused on the surface of flat commercial soda-lime silicate glass substrates.

Silicon micromachining is a very important technology in microfabrication and microelectromechanical system (MEMS) industry. Nd:YAG laser has a wavelength of 1.06 μm, which is adsorbed by silicon, and is easily used for direct silicon machining. But the cost is very high. Although CO_2 laser is cheap, its wavelength of 10.64 μm is not absorbed by silicon. However, a silicon sample put on the top of a glass, instead of pure silicon, is used for CO_2 laser micromachining. The silicon on the top of a glass may absorb the CO_2 laser and become able to be etched, even through the wafer. Commercial available air-cooled CO_2 laser equipment can be used with a maximum laser power of 30 W. A glass below the silicon changes the absorption of silicon to CO_2 laser during machining. The silicon on the top of a glass may be etched by CO_2 laser even through the wafer due to the absorption variation. The etching depth increases with the pass number at constant laser power and scanning speed.

Several techniques are available that allow the size distribution of an aerosol to be determined in real time, but the determination of chemical composition, which has traditionally been done by impaction methods, is slow and yields only an average composition of the ensemble of particles in a given size range. It is essential, therefore, that new techniques be developed to allow the characterization of both the physical properties and chemical composition of aerosols, and that these operate on a time-scale that allows changes in the aerosol composition to be determined in real time. Several variants of the aerosol TOFMS (ATOFMS) instrument have been described in the literature [2]. The principle of the most sophisticated instrument reported to date employs two laser systems; first, a tuneable IR laser (OPO) is used to desorb material selectively from the particle, and then a second (VUV) laser is used to ionize the molecules that are produced [2]. With this approach, greater control over the particle ablation and ionization steps is possible, and by using low IR laser energy for the first evaporation step it is possible to depth profile heterogeneously mixed aerosol particles. Molecular information can be obtained by tuning the laser energy to just above the threshold required for desorption.

5. Conclusions

Several applications have been demonstrated for CO_2 lasers, despite it is impossible to use photoelectric emission to detect this radiation (photon energy of about 0.1 eV is only about five times room temperature, and cryogenically cooled photoconductors are necessary to achieve fast low-level detection) and little engineering has been done in the mid-infrared region.

All applications mentioned require a stable, single-frequency source of radiation. A kilowatt of radiation at 10 microns, focused down to its diffraction limit, is a power density of 1 gigawatt per square cm. Because most materials absorb at 10 microns, considerable interest has been shown in CO_2 lasers in many applications, and any problem which requires controlled surface heating or burning might find a potential solution with the CO_2 laser.

The MTL3-GT CO_2 laser ability to combine the laser pulsed mode with tune-ability introduces new perspectives to perform different experiments, which require a suitable, reliable and user-friendly procedure. With the method described in this work, many experiments can be performed in real time with simultaneous control of power/energy and wavelength, and taking advantage of the full laser power for each selected wavelength. One could observe, after improving the procedure, that energy values are more stable in all four emission bands (9P, 9R, 10P and 10R). This behavior was also observed regardless of the repetition rate, even for higher ones around 100 Hz. Besides energy, power was also measured and improved following the same procedure. This procedure can also be used on other infrared lasers with some minor adaptations regarding the software and energy detectors used. The observation of the energy line variation in real time is very important for understanding the behavior of the laser under certain external conditions and also to make sure that internal mechanisms are also error free.

It was demonstrated that CO_2 laser applications in the fields of nanoscience and nanotechnology are very promising, with particular relevance on spectroscopy, photodynamic kinetics and photodynamic therapy, ultra-pure and size-selected

nanoparticle production, surgery and biomedicine, nanoanalysis, nanomaterials processing and composite nano-engineered catalysts.

6. References

[1] W. Demtröder, *Laser Spectroscopy*, 3rd Ed. Springer, 2003.
[2] H. H. Telle, A. Gonzalez Ureña, R. J. Donovan, *Laser chemistry,* Wiley, (2007).
[3] C. N. Patel, *Phys. Rev. Lett.* 12 (1964) 588.
[4] A. J. Beaulieu *Appl. Phys. Lett.* 16 (1970) 504.
[5] J. F. Ribeiro and R. F. M. Lobo, *Eur. J. Phys.* 30 (2009) 911.
[6] Edinburgh Instruments Ltd, *TEA CO2 MTL3-GT Laser User's Manual*, Issue G September, 2003.
[7] G. Scoles, *Atomic and Molecular Beam Methods* , Oxford University Press, New York, 1992.
[8] J. Steinfeld, *Laser-Induced Chemical Processes*, Plenum Press, New York, 1981.
[9] C. Miller, R. Zare, *Chem. Phys. Lett*., 71 (1980) 376.
[10] M. Bronikowski, W. Simpson, R. Zare, *J. Phys. Chem.* 97 (1992) 2194.
[11] Z. Liu, *Science* 312 (2006) 1024.
[12] Y. T. Lee, Y. R. Shen, *Phys. Today* 33 (1980) 11.
[13] W. Gardiner, *Combustion Chemistry*, Springer, New York, 1994.
[14] J. Warnatz, U. Maas, R. Dibble, *Combustion*, Springer, Heidelberg, 1996.
[15] M. J. Shultz, E. J. Rock, R. E. Tricca, L. M. J. Yam, *Phys. Chem.* 88 (1984) 5157.
[20] I. Herman, *Chem. Rev.* 89 (1989) 1323.
[16] J. Castano, V. Zapata, G. Makarov and A. Gonzalez Urena, *J. Phys. Chem.* 99 (1995) 13659.
[17] Friedrich Huisken, Martin Stemmler, *Chem. Phys.Lett.* 144 (1988) 391.
[18] M. Köllner, *Appl. Opt.*, 32 (1993) 806.
[19] C. Liang, Y. Shimizu, T. Sasaki, N. Koshisaki, *J. Mater. Res*, 19 (2004) 1551.
[20] I. Herman, *Chem. Rev.* 89 (1989) 1323.
[21] M. Ehbrecht and F. Huisken, *Phys. Rev. B*, 59 (1999) 2975.
[22] G. Ledoux, R. Lobo, F. Huisken, O. Guillois, C. Reynaud, *Photoluminescence of Silicon Nanocrystals Synthetised by Laser Pyrolysis*, in Trends in Nanotechnology Research, ed. E. Dirote, Nova Siience Publish, New York, 2004.
[23] B. Bhushan, *Handbook of Nanotechnology*, Springer, New York, 2004.
[24] N. Kouklin, M. Tzolov, D. Straus, A. Yin, and J. M. Xu, *Appl. Phys. Lett.* 85 (2004) 4463.
[25] L. Zhang, V. U. Kiny, H. Peng, J. Zhu, R.F.M. Lobo, J. L. Margrave, V. N. Khabashesku, *Chem. Mat*., 16 (2004) 2055.
[26] W. Maser, A M Benito, E Munoz, G M de Val, M T Martınez, A Larrea and G de la Fuente, *Nanotechnology* 12 (2001) 147.
[27] R. Alexandrescu, A. Crunteanu, R.-E. Morjan, I. Morjan, F. Rohmund, L. Falk , G. Ledoux, F. Huisken, *Infrared Physics & Technology* 44 (2003) 43.
[28] I. Morjan, I. Soare, R. Alexandrescu, L. Gavrila-Florescu, R Morjan, G. Prodan, C. Fleaca, I. Sandu, I. Voicu , F. Dumitrache, E. Popovici, *Infrared Physics & Technology* 51 (2008) 186.
[29] M. S. Castro, E. D. Sam, M. Veith and P. W. Oliveira, *Nanotechnology* 19 (2008) 105704.
[30] S.I. Klink, H. Keizer and V. Veggel, *Angewandte Chemie International Edition* 39 (2000) 4319.
[31] Y. Guo, M. Kumar and P. Zhang, *Chem. Mater. 19* (2007) 6071.

[32] F. J. M. Harren and J. Reuss, *Photoacoustic Spectroscopy* in Encyclopedia of Applied Physics, vol 19, G L Trigg (ed.) , VCH, Weinheim,1997.
[33] M. W. Sigrist, A. Bohren, T. Lerber, M. Nagel, M. Romann, *Anal. Sci.*, 17 (2001) S511.
[34] De Vries, F J M Harren and J Reuss, *Biol. Technol.*, 6 (1995) 275.
[35] J. M. Orea, C. Montero, J. B. Jiménez, A. G. Ureña, *Anal Chem.*, 73 (2001) 5921.
[36] C. Montero, J. M. Orea, M. Soledad Muñoz, R. F. M. Lobo, A. González Ureña, *Applied Phys. B*, 71 (2000) 601.

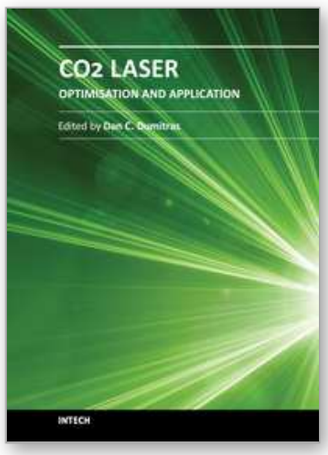

CO2 Laser - Optimisation and Application

Edited by Dr. Dan C. Dumitras

ISBN 978-953-51-0351-6
Hard cover, 436 pages
Publisher InTech
Published online 21, March, 2012
Published in print edition March, 2012

The present book includes several contributions aiming a deeper understanding of the basic processes in the operation of CO2 lasers (lasing on non-traditional bands, frequency stabilization, photoacoustic spectroscopy) and achievement of new systems (CO2 lasers generating ultrashort pulses or high average power, lasers based on diffusion cooled V-fold geometry, transmission of IR radiation through hollow core microstructured fibers). The second part of the book is dedicated to applications in material processing (heat treatment, welding, synthesis of new materials, micro fluidics) and in medicine (clinical applications, dentistry, non-ablative therapy, acceleration of protons for cancer treatment).

INTECH
open science | open minds

InTech Europe
University Campus STeP Ri
Slavka Krautzeka 83/A
51000 Rijeka, Croatia
Phone: +385 (51) 770 447
Fax: +385 (51) 686 166
www.intechopen.com

InTech China
Unit 405, Office Block, Hotel Equatorial Shanghai
No.65, Yan An Road (West), Shanghai, 200040, China
中国上海市延安西路65号上海国际贵都大饭店办公楼405单元
Phone: +86-21-62489820
Fax: +86-21-62489821

IntechOpen